



http://pubs.acs.org/iournal/aesccg

Article

Gas-Phase Reaction Kinetics of the Ortho and Ipso Adducts 1,2,4,5-Tetramethylbenzene—OH with O_2

Paulo Alarcón, Birger Bohn,* Thomas Berkemeier, Gerhard Lammel, Ulrich Pöschl, and Cornelius Zetzsch*



Cite This: ACS Earth Space Chem. 2021, 5, 2243-2251



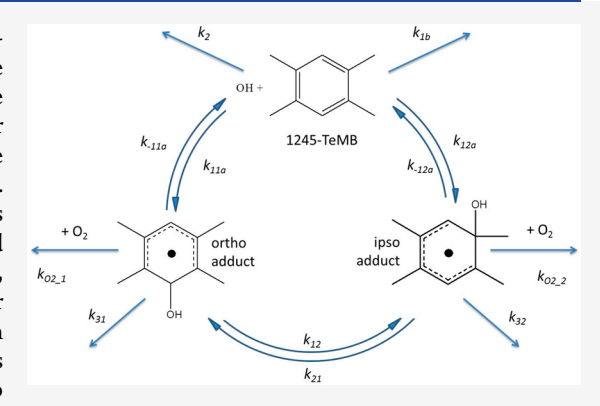
ACCESS

III Metrics & More

Article Recommendations

SI Supporting Information

ABSTRACT: The reversible reaction of OH radicals with 1,2,4,5-tetramethylbenzene (1245-TeMB, durene) leads to adducts at the substituted (ipso) and unsubstituted (ortho) positions of the ring. By the use of flash photolysis for production and resonance fluorescence for detection of OH, the gas-phase reactions of O_2 with these adducts were investigated over the temperature range of 300–340 K in He at 200 mbar. The decay of OH, generated by pulsed vacuum-UV photolysis of H_2O , was monitored under slow-flow conditions in the presence of 1245-TeMB and O_2 at concentrations of up to 19×10^{12} cm⁻³ and 2×10^{16} cm⁻³, respectively. Triexponential OH decays resulted from the unimolecular decomposition of the two adducts, representing OH reservoirs with different stabilities. In the presence of O_2 , additional adduct loss pathways exist, leading to faster OH consumption. Triexponential functions fitted to these decays were analyzed to obtain rate constants for the reactions of O_2



with both adducts. Rate constants in the range of $(4-13) \times 10^{-15}$ and $(0.3-3) \times 10^{-15}$ cm³ s⁻¹ were obtained for the ortho and the ipso adducts, respectively, depending on temperature and assumptions regarding details of the underlying mechanism of adduct isomer formation and isomerization. At O₂ concentrations exceeding about 1×10^{16} cm⁻³, deviations from a linear dependence of the adduct loss rates on the O₂ concentration indicate an even more complex mechanism. The validity of the rate constants is therefore confined to O₂ concentrations below 1×10^{16} cm⁻³. The adduct + O₂ rate constants for 1245-TeMB are greater than the corresponding previously obtained rate constants for benzene, toluene, and *p*- and *m*-xylene but smaller than those for hexamethylbenzene. The results are discussed in terms of the current knowledge about the mechanism of OH-induced degradation of aromatic compounds in the presence of O₂.

KEYWORDS: OH radical, aromatic compounds, atmospheric chemistry, photochemistry, gas-phase kinetics

■ INTRODUCTION

Non-methane volatile organic compounds (NMVOCs) enter the atmosphere from anthropogenic and biogenic sources. On a global scale, emissions from biogenic sources exceed those from anthropogenic origin. However, anthropogenic emissions can be predominant on a regional scale in urbanized areas.² Aromatic compounds are an important group of anthropogenic NMVOCs. Their oxidation in the atmosphere finally leads to the formation of tropospheric ozone and precursors of secondary organic aerosol. 3,4 A detailed knowledge of the underlying oxidation mechanisms therefore helps in understanding the impact of this class of NMVOCs on urban air quality. Moreover, some aspects of the oxidation mechanisms of aromatics are of general interest for atmospheric chemistry because they involve the reversible formation of peroxy radicals, which are relevant for VOCs like isoprene,6 as well as intramolecular reactions of peroxy radicals related to autoxidation processes and the formation of highly oxidized molecules.

Monocyclic aromatic hydrocarbons with varying degrees of methylation react with OH radicals with rate constants ranging from $1.2\times 10^{-12}~{\rm cm}^3~{\rm s}^{-1}$ for unsubstituted benzene to $1.5\times 10^{-10}~{\rm cm}^3~{\rm s}^{-1}$ for fully substituted hexamethylbenzene at 298 K. $^{9-15}$ For 1,2,4,5-tetramethylbenzene (1245-TeMB), rate constants of around $5.8\times 10^{-11}~{\rm cm}^3~{\rm s}^{-1}$ were determined previously 14,15 with a slightly negative temperature coefficient B in $k_{\rm OH}=A\exp(-B/T)$. The major OH reaction pathway at atmospheric temperatures is addition to the aromatic ring, while H atom abstraction from CH₃ substituents is minor, accounting for about 11% of the total rate constant for the monosubstituted derivative toluene at room temperature. 9

Special Issue: Mario Molina Memorial

Received: June 26, 2021 Revised: August 9, 2021 Accepted: August 15, 2021 Published: August 27, 2021





With increasing methylation, the importance of abstraction reactions decreases to around 4% for 1245-TeMB¹⁴ because activation of the addition pathway by the substituents is dominant.^{3,9}

A special feature of additions of OH to aromatics is that these reactions are reversible because of the strength of the aromatic bonds. While the reversibility has virtually no consequences for the atmospheric degradation of aromatics because of rapid consecutive O2 reactions under tropospheric conditions, it opens the possibility to study the kinetics of OH—aromatic adducts in pulsed experiments in the laboratory. Decay curves of OH in the presence of aromatics ideally become biexponential as a result of the reversible addition. 16-18 In the presence of adduct scavengers like O2, the OH decays remain biexponential but change in a distinctive way from which the rate constants of the adduct + O2 reactions can be inferred. With this method, the rate constants of adduct reactions with O₂ (and other scavengers) were determined for several aromatic compounds, albeit confined to relatively low concentrations of O_2 . The results cover a wide range of rate constants from around 2×10^{-16} cm³ s⁻¹ for benzene to 2×10^{-16} 10⁻¹³ cm³ s⁻¹ for hexamethylbenzene with little, if any, temperature dependence in the range 300-360 K.^{17,18}

Direct detection of OH—aromatic adducts by UV absorption provided additional insight into the adduct kinetics at elevated O_2 concentrations. With this method, clear evidence for a complex mechanism with fast reversible formation of peroxy radicals and competing unimolecular or bimolecular loss reactions was found for benzene and toluene. 19–23 Qualitatively, the reversibility of the O_2 addition is again explainable by the high stability of the OH adduct with two conjugated double bonds. For the rate constants obtained at low O_2 concentrations, the complex mechanism implies that they are effectively second-order and cannot be assigned to elementary adduct + O_2 reactions. This conclusion is in qualitative agreement with available theoretical work. O_2

The formation of adduct isomers in the OH + aromatic reactions is another challenge for the investigation of adduct kinetics. Several isomers can be formed, including ipso isomers, where OH adds at already-substituted positions on the aromatic ring, $^{26-28}$ apart from stereoisomers. Deviations from biexponential OH decay behavior were observed for several aromatic compounds in a narrow temperature range between about 300 and 340 K, and an evaluation scheme for the analysis of triexponential OH decay curves was developed and applied in previous work. This scheme is strictly applicable when two isomers are formed and can be extended to investigate the kinetic behavior of the adduct isomers in the presence of scavengers like O_2 .

In this work, the rate constants for the reactions of O_2 with the ortho and ipso isomers of 1245-TeMB—OH adducts were determined. 1245-TeMB was selected because the triexponential behavior of the OH decay was distinctive in previous work. Even though the exact mechanism of adduct isomer formation through OH addition and possible isomerization reactions remained unclear, the ortho isomer was tentatively identified to be formed preferentially and to decompose more readily back to OH. The ipso isomer was characterized by smaller decomposition rate constants, which make it more elusive at lower temperatures. These assumptions are adopted in the following to assign the kinetic properties of the isomers toward O_2 .

■ EXPERIMENTAL SECTION

The experimental setup has been described in detail elsewhere. 16,18,30 Briefly, OH radicals were generated by pulsed vacuum-UV flash photolysis of water vapor in a reaction cell using a flash lamp with a MgF₂ window (PerkinElmer FX 1165, operated above typical specifications, with a flash energy of 540 mJ). The OH in the reaction cell was excited electronically by radiation from a resonance lamp mounted at an angle of 90° with respect to the photolysis beam. A gas mixture of He and H₂O (at a total pressure of 200 mbar) flowed through the resonance lamp, where a microwave discharge dissociated H₂O to produce $OH(A^2\Sigma^+)$, the emission of which was focused into the reaction cell. The resonance fluorescence emitted by the OH radicals in the cell passed through a 308 nm interference filter at right angles to the photolysis beam and the resonance lamp and was focused onto the photocathode of a photomultiplier tube and monitored by photon counting for 5 s after each flash. The counts were accumulated by multichannel scaling using a dwell time of 0.977 ms and averaged over 40 decays. Moreover, a data compression algorithm was applied to improve the manageability of the raw data. The total He pressure and the concentration of water vapor in the cell were kept constant at 200 mbar and 1.5×10^{15} cm⁻³, respectively. The temperature in the cell was varied between 299 and 339 K. The oxygen and 1245-TeMB concentrations were varied between 1×10^{15} and 20×10^{15} cm⁻³ and between 5×10^{12} and 20×10^{12} cm⁻³, respectively. Four different 1245-TeMB concentrations were used, while the O2 concentration was varied in smaller steps of 1×10^{15} cm⁻³. The conditions were chosen to produce evaluable triexponential OH decays that were suitable for the time resolution of the detection system.

The gases used in this work had the following minimum purities stated by the manufacturers: He (Westfalen AG), >99.9999%; N_2 (Westfalen AG), >99.9999%; O_2 (Westfalen AG), >99.9999%. Solid 1245-TeMB (Aldrich, >98%) was further purified by sublimation under vacuum at 70 °C.

■ RESULTS AND DISCUSSION

Reaction Mechanism and Data Analysis. The mechanism for the reaction of OH radicals with selected aromatic compounds leading to the formation of two adduct isomers, which produce triexponential OH decay curves, was devised previously. In the present work, this mechanism was extended by the two adduct + O_2 reactions for 1245-TeMB as shown in Figure 1. The reaction scheme can be summarized by reactions 1–9. It should be noted that reactions 1–3 are reversible.

OH + 1245-TeMB
$$\underset{k_{-11a}}{\overset{k_{11a}}{\Longleftrightarrow}}$$
 ortho adduct (1)

OH + 1245-TeMB
$$\stackrel{k_{12a}}{\Longleftrightarrow}$$
 ipso adduct (2)

ortho adduct
$$\underset{k_{21}}{\overset{k_{12}}{\rightleftharpoons}}$$
 ipso adduct (3)

OH + 1245-TeMB
$$\stackrel{k_{1b}}{\rightarrow}$$
 products (4)

OH (+ R)
$$\stackrel{k_2}{\rightarrow}$$
 products (5)

ortho adduct
$$(+R) \xrightarrow{k_{31}}$$
 products (6)

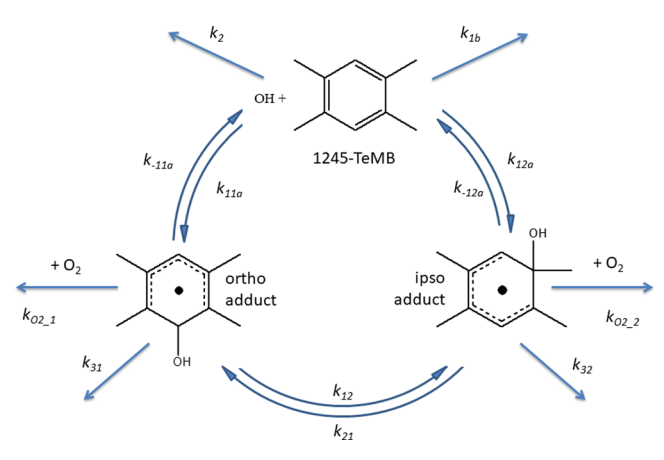


Figure 1. Mechanism for the reaction of OH radicals with 1245-TeMB in the presence of O₂. k_2 , k_{31} , and k_{32} are first-order rate constants of unspecified irreversible losses of OH and the two adducts. k_{1b} is the rate constant for the OH + 1245-TeMB H-abstraction reaction (no OH re-formation).

ipso adduct
$$(+R) \xrightarrow{k_{32}}$$
 products (7)

ortho adduct +
$$O_2 \xrightarrow{k_{O2,1}} \text{products}$$
 (8)

ipso adduct +
$$O_2 \xrightarrow{k_{O2,2}}$$
 products (9)

The additional reactions 8 and 9 do not change the general solutions for the differential equation system corresponding to reactions 1–7. Details regarding these solutions and the parameters that can finally be determined in a simultaneous analysis of sets of experimental OH decay curves by specially adapted fitting procedures will not be repeated here. These have been presented in our previous publications. ^{15,29} Main results relevant for the determination of the rate constants of reactions 8 and 9 are summarized in the following.

Already in the absence of O2, no unique set of the 10 rate constants introduced in reactions 1-7 can be determined, for the following reasons: First, some of the rate constants in the solutions appear as products or sums that cannot be separated, resulting in seven fit parameters related to the reaction rate constants. Second, one more fit parameter is required than there are terms available that define the sets of triexponential OH decays with two amplitude ratios and three decay rate constants for each curve. To solve this problem of underdetermination, two special cases of the reaction mechanism were defined in which the number of fit parameters is reduced by one. These limiting cases of the full mechanism are called cases A and B in the following and correspond to our former notations model-2 and model-3 in a different context. 15,29 Cases A and B produce the same decay curves but are defined by different fit parameters. For case A, the rate constants of the adduct isomerization reactions, k_{12} and k_{21} (Figure 1, bottom), were set to zero, and the following fit parameters were determined: k_2 , $k_{\text{OH}} = [k_{11a} + k_{12a} + k_{1b}]$, $[k_{11a} \times k_{-11a}]$, $[k_{12a} \times k_{-11a}]$ k_{-12a}], $k_{L_{-1}} = [k_{-11a} + k_{31}]$, and $k_{L_{-2}} = [k_{-12a} + k_{32}]$. For case B, the rate constants for the direct formation and decomposition of the ipso adduct, k_{12a} and k_{-12a} (Figure 1, right), were set to zero, which led to the following parameters: k_2 , $k_{OH} = [k_{11a} +$ $k_{12a}+k_{1b}$], $[k_{11a}\times k_{-11a}]$, $[k_{12}\times k_{21}]$, $k_{L_{-1}}=[k_{-11a}+k_{12}+k_{31}]$, and $k_{L_{-2}}=[k_{21}+k_{32}]$. Only two fit parameters turned out to be the same in both cases, namely, k_2 and k_{OH} , which fixed the total loss rate constant of OH, $k_{\text{L OH}} = k_2 + k_{\text{OH}}$. Moreover, it

was shown that for intermediate cases, i.e., when $k_{12} \times k_{21} \cap k_{12a} \times k_{-12a} \neq 0$, the other fit parameters range within the limits obtained for cases A and B. ¹⁵

Inclusion of the two O2 reactions was achieved by extending the total loss rate constants of the adduct isomers, $k_{\rm L-1}$ and k_{L_2} : for case A, $k_{L_1} = k_{-11a} + k_{31} + k_{O2_1}[O_2]$ (ortho adduct) and $k_{L 2} = k_{-12a} + k_{32} + k_{O2} _{2}[O_{2}]$ (ipso adduct); for case B, procedures were adapted to allow for simultaneous evaluation of the decay curves obtained at various aromatic and O2 concentrations, directly returning the rate constants for the reactions of O2 with both adducts for case A or case B. No constraints were applied in the fits, but starting values of the fit parameters were estimated from exponential prefits to single curves (starting values and backgrounds)²⁹ and from results in the absence of O₂. In order to illustrate the method and the dependence of the decay rate constants and amplitude ratios on the experimental conditions and the total loss rate constants of the three species involved, we show some examples in the Supporting Information.

Several tests were performed to investigate the consistency of the fit results in the presence and absence of O_2 . For this purpose, fit quality was determined by the sum of squared residuals (χ^2) divided by the number of degrees of freedom (DOF), i.e., the number of data points minus the number of fitted parameters. Moreover, uncertainties in the fitted parameters were estimated by a sensitivity analysis using a bootstrap method: from a given set of N decay curves, new sets of N decay curves for the fits were selected randomly (resampling with replacement). This was repeated 100 times to obtain mean values and standard deviations of fitted parameters and fit qualities.³¹

To test the analytical method applied in this study, we also used an explicit numerical model that included the full reaction mechanism and was coupled to a global optimization algorithm.³² The numerical model can operate beyond the limiting cases A and B and allows the reaction mechanism to be extended, if necessary. The preliminary results from free fits to the measurement data are consistent with the analytical model and will be presented in detail in a follow-up study.

Results. Figure 2 shows an example of OH decays obtained at a fixed 1245-TeMB concentration with different O2 concentrations at constant temperature. As expected, the decay of OH gets faster with increasing O2 concentration, which is caused by losses of adducts from the equilibria (i.e., reactions 8 and 9). In the Supporting Information we show a linear representation of Figure 2 with corresponding residuals. The full and dashed lines show the corresponding fits to cases A and B of the mechanism, respectively. In this example, for clarity only five of the 87 simultaneously fitted OH decay curves are shown. There are small differences between the full and the dashed curves, which means that cases A and B no longer result in the same OH decays compared with our previous study.¹⁵ However, the differences are insignificant, which is also reflected in the very similar fit qualities for both cases, as explained in more detail in the following.

Although the number of decay curves without O_2 was rather limited, an analysis of these decay data alone was feasible. It returned the parameters for cases A and B within reasonable agreement with our previous study on 1245-TeMB. More details of this comparison are given in the Supporting Information. Moreover, χ^2/DOF ratios of around unity

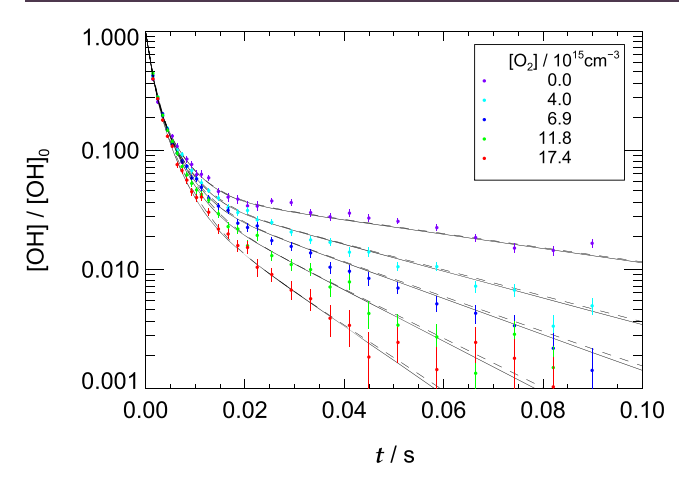


Figure 2. Normalized OH decay curves obtained at 330.3 K, a 1245-TeMB concentration of 1.38×10^{13} cm⁻³, and selected O_2 concentrations increasing from top to bottom and given in the inset. Full and dashed lines show the corresponding fit results according to cases A and B, respectively, where a total of 87 OH decay curves at different 1245-TeMB and O_2 concentrations were considered.

indicated that the uncertainties of the data points were considered correctly and that the underlying model is applicable in the absence of O_2 . When OH decay curves obtained in the presence of O_2 were included in the analysis, the rate constants for the O_2 reactions (reactions 8 and 9) were returned as intended, but the fit qualities were significantly poorer, as listed in Table 1. In addition, some of the other parameters that should not be affected by the presence of O_2 were different and outside the estimated uncertainties. This indicates that the assumed mechanism is not fully consistent with the experimental data.

To investigate the reason for the poorer fit qualities in more detail, the OH decay curves obtained in the presence of $\rm O_2$ were binned into $\rm O_2$ concentration increments of $\rm 0.5 \times 10^{15}$ cm⁻³. The selected curves (typically three or four per bin) were then evaluated together with those without $\rm O_2$ to obtain $\rm O_2$ loss rate constants as functions of $\rm O_2$ in a two-point approach. Ideally, this should result in linear dependences of the adduct loss rates on the $\rm O_2$ concentrations with slopes corresponding to the second-order rate constants $k_{\rm O2_1}$ and $k_{\rm O2_2}$. An example for case A and case B fit results at a temperature of 330 K is shown in Figure 3. The expected linearity is apparently limited to low $\rm O_2$ concentrations below

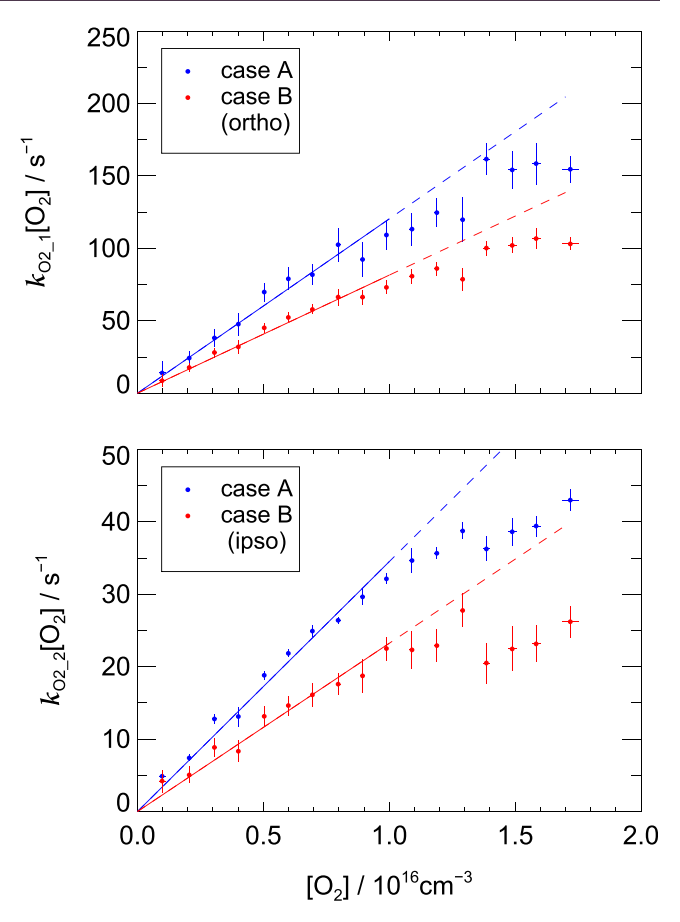


Figure 3. First-order adduct loss rate constants as functions of the O_2 concentration from combined fits to OH decay curves in the absence of O_2 and at O_2 concentrations within $\pm 0.5 \times 10^{15}$ cm⁻³ of the plotted values: (top) ortho adduct; (bottom) ipso adduct. This example was obtained at a temperature of 330.3 K. Solid lines and dashed extrapolations show linear regression results in the range $[O_2]$ < 1×10^{16} cm⁻³ that were forced through the origin. Error bars are standard deviations from the bootstrap analysis.

about 1×10^{16} cm⁻³ for both adduct isomers, as indicated by the solid lines and dashed extrapolations. Qualitatively similar behavior was found for the other temperatures but was less regular for lower temperatures, especially for the ipso isomer and case B. All of the other parameters and fit qualities remained in reasonable agreement with those obtained in the absence of O_2 . Corresponding plots for other kinetic

Table 1. Fit Qualities χ^2/DOF and Their Standard Deviations from a Bootstrap Analysis Obtained from Simultaneous Fits to Isothermal Sets of OH Decay Curves at Different Temperatures^a

	$\chi^2/{\rm DOF}$ (OH decays without O ₂)			χ^2/DOF (all OH decays)			
T/K	N	case A	case B	N	case A	case B	
299.3	7	1.02 ± 0.08	1.02 ± 0.07	82	-	1.19 ± 0.03	
309.3	5	1.04 ± 0.05	1.05 ± 0.04	62	1.20 ± 0.04	1.20 ± 0.04	
316.6	5	0.89 ± 0.07	0.90 ± 0.07	64	1.37 ± 0.07	1.44 ± 0.08	
319.3	7	0.99 ± 0.05	1.00 ± 0.05	87	1.36 ± 0.06	1.43 ± 0.07	
323.5	5	1.08 ± 0.09	1.08 ± 0.09	64	1.42 ± 0.07	1.51 ± 0.09	
330.4	7	1.17 ± 0.07	1.17 ± 0.06	87	1.33 ± 0.04	1.38 ± 0.05	
339.3	9	1.07 ± 0.05	1.07 ± 0.05	118	1.55 ± 0.05	_	

^aThe fit qualities are identical for cases A and B in the absence of O_2 (left) and within the estimated uncertainties in the presence of O_2 (right) but significantly poorer for all temperatures when curves in the presence of O_2 were included. Where no numbers are given, the fits returned no positive results for all parameters.

Table 2. Rate Constants $k_{\rm O2_1}$ and $k_{\rm O2_2}$ and Fit Qualities $\chi^2/{\rm DOF}$ with Standard Deviations from a Bootstrap Analysis of Simultaneous Fits to Isothermal Sets of OH Decay Curves at Different Temperatures with $[{\rm O_2}] < 1 \times 10^{16}~{\rm cm}^{-3}$ Obtained for Cases A and B

	$k/10^{-15} \text{ cm}^3 \text{ s}^{-1} \text{ (case A)}$			<i>k</i> ,			
T/K	k _{O2_1} (ortho)	$k_{\rm O2_2}~({\rm ipso})$	χ²/DOF	k _{O2_1} (ortho)	k _{O2_2} (ipso)	χ²/DOF	N
299.3	5.6 ± 1.7	2.1 ± 0.7	1.11 ± 0.04	4.2 ± 1.0	1.2 ± 1.1	1.11 ± 0.04	42
309.3	8.3 ± 0.5	1.5 ± 0.3	1.16 ± 0.06	6.2 ± 0.4	0.3 ± 0.3	1.14 ± 0.05	33
316.6	11.0 ± 0.7	2.3 ± 0.2	1.17 ± 0.06	7.8 ± 0.5	0.6 ± 0.2	1.22 ± 0.07	34
319.3	11.7 ± 0.4	2.6 ± 0.3	1.18 ± 0.04	8.1 ± 0.3	0.9 ± 0.4	1.24 ± 0.05	47
323.5	12.2 ± 0.8	2.8 ± 0.2	1.19 ± 0.06	7.9 ± 0.5	1.5 ± 0.3	1.25 ± 0.07	34
330.4	11.1 ± 0.8	3.4 ± 0.1	1.19 ± 0.05	7.3 ± 0.4	2.4 ± 0.2	1.21 ± 0.04	47
339.3	13.4 ± 3.9	2.1 ± 1.0	1.49 ± 0.08	9.3 ± 0.7	1.2 ± 0.5	1.48 ± 0.07	57

parameters of this example can be found in the Figures S6 and S7

As expected, simultaneous fits of all of the OH decay curves with $[{\rm O}_2] < 1 \times 10^{16}~{\rm cm}^{-3}$ resulted in improved fit qualities and significantly greater ${\rm O}_2$ rate constants compared with the analysis including all of the OH decay curves. The finally derived rate constants and fit qualities are listed in Table 2. The fit qualities are still very similar for cases A and B. The rate constants $k_{{\rm O}_2-1}$ and $k_{{\rm O}_2-2}$ differ significantly for the two cases at all temperatures, with the case B rate constants being smaller than those for case A. Because neither case A nor case B can be excluded, the rate constants for both isomers could range somewhere between the case A and case B results. Nevertheless, a clear difference between the isomers remains, with greater adduct + ${\rm O}_2$ rate constants for the ortho isomer (i.e., $k_{{\rm O}_2-1} > k_{{\rm O}_2-2}$).

It should be noted that the qualities of these final fits that were confined to lower maximum O_2 concentrations are still poorer than those in the absence of O_2 and for the subsets evaluated to determine the O_2 concentration dependence in the preceding paragraph. The adduct + O_2 rate constants are also slightly smaller than those corresponding to the solid lines forced through the origin shown in Figure 3. This indicates that even in the low O_2 concentration range some deviations from the proposed mechanism may still exist. However, the differences in the O_2 rate constants are small and within the estimated uncertainties.

Discussion. Figure 4 shows an Arrhenius plot of the adduct + O₂ rate constants for the ortho and ipso isomers of 1245-TeMB-OH. The error bars cover the case A and case B data including standard deviations listed in Table 2, with case A corresponding to the upper limits and case B to the lower limits. Overall, for the two isomers a similar small positive temperature dependence results, with a temperature coefficient B of \sim 2000 K, as indicated by the solid lines. Also shown in Figure 4 are temperature-dependent adduct + O2 reaction rate constant data for benzene, toluene, p-xylene, and m-xylene reported by Koch et al. in 2007, 18 for which no or little temperature dependence of the rate constants was found as well. The small increase with temperature in the case of benzene corresponds to that derived in this work for 1245-TeMB. The Arrhenius parameters that reproduce the straight lines in Figure 4 are listed in Table 3. Moreover, the general tendency of increasing rate constants with increasing degree of methylation is confirmed by 1245-TeMB. Koch et al. 18 also determined the adduct + O2 rate constants for hexamethylbenzene at elevated temperatures of up to 385 K, which were necessary to obtain an appreciable dissociation of the corresponding very stable ipso adduct. Those adduct + O₂

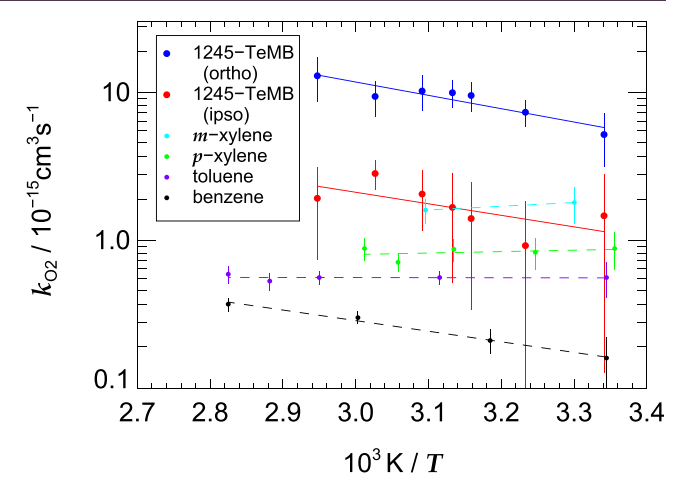


Figure 4. Arrhenius plots of rate constants for the reactions of the ortho and ipso 1245-TeMB-OH adduct isomers with O $_2$ in comparison with rate constants for OH adducts with benzene, toluene, *p*-xylene, and *m*-xylene from the literature. ¹⁸ The error bars for the ortho and ipso isomers cover the maximum and minimum values obtained for cases A and B including standard deviations, as listed in Table 2. The Arrhenius parameters corresponding to the straight lines are listed in Table 3.

rate constants were much larger than for the other aromatic compounds (1.8×10^{-13} and 1.2×10^{-13} cm³ s⁻¹ at 355 and 385 K, respectively; for clarity, these are not included in Figure 4).

Koch et al. ¹⁸ used the same instrument and applied a similar analysis technique as in this work, but they did not consider adduct isomers in their analysis because no deviation from biexponential OH decay behavior was observed. At least for p-xylene, this is in slight contradiction with the work by Alarcón et al. reported in 2015, ¹⁵ where triexponential OH decays were identified for this compound, pointing toward the formation of ipso adduct isomers. In any case, the results shown in Figure 4 are expected to be dominated by the properties of the ortho adducts for toluene, p-xylene, and m-xylene. The two aromatic compounds that cannot form adduct isomers, benzene and hexamethylbenzene, clearly define the lower and upper limits of the adduct + O_2 rate constants reported to date.

The relative yields of OH adduct isomers from different monoaromatics are still uncertain. There is merely indirect experimental evidence for the presence of different isomers, as presented in this and previous work. Specifically for 1245-TeMB, an ipso isomer yield > 9% was derived indirectly in a product study under atmospheric conditions. Adduct isomer yields for several aromatic compounds were determined in

Table 3. Arrhenius Parameters A and B for Effective OH Adduct + O_2 Rate Constants k_{O_2} for Different Methylated Monocyclic Aromatics Applicable within the Given Temperature and O_2 Concentration Ranges^a

compound	T/K	$[O_2]/10^{16} cm^{-3}$	$A/\text{cm}^3 \text{ s}^{-1}$	B/K	Reference ^b
benzene	299-354	0-10	3.0×10^{-14}	1600	18
toluene	299-354	0-5	5.8×10^{-16}	0	18
p-xylene	298-332	0-2	4.1×10^{-16}	-220	18
m-xylene	303-323 ^c	0-2	2.7×10^{-16}	-580	18
hexamethylbenzene	355-385 ^c	0-0.04	9.9×10^{-16}	-1850	18
1245-TeMB (ortho)	299-339	0-1	6.0×10^{-12}	2100	this work
1245-TeMB (ipso)	299-339	0-1	4.6×10^{-13}	1800	this work

^aThe values of A and B were derived from unweighted fits of the logarithms of the expression $k_{O_2} = A \exp(-B/T)$. ^bData from room-temperature studies discussed in the text were not included. ^cOnly two temperatures were available.

theoretical studies but with partly conflicting results. In this context, we refer to a recent review of theoretical work on the atmospheric oxidation of aromatic compounds by Vereecken. Overall, no conclusive picture has emerged from the theoretical studies except that ortho isomers are generally preferred because the methyl substituents stabilize the conjugated cyclohexadienyl radical. Moreover, whether isomerization reactions between the adduct isomers (with rate constants k_{12} and k_{21}) can occur has to our knowledge not yet been investigated theoretically; these reactions have been included in the mechanism (Figure 1) more for formal reasons than for chemical intuition. Therefore, we cannot further confine our results for the adduct + O_2 rate constants with a clear preference for either case A or case B of the general mechanism.

The OH adduct + O₂ rate constants for benzene and toluene around 300 K were confirmed in studies utilizing direct detection of adducts by UV absorption. ^{19–21,23} In those studies, the adduct decay rates were observed to level off at elevated O_2 concentrations exceeding about 1×10^{18} cm⁻³ and approached saturation at $[O_2] > 2.5 \times 10^{19} \text{ cm}^{-3}$. This behavior is consistent with the fast, reversible formation of a peroxy radical in the adduct + O2 reaction, competing with other, slow bimolecular loss reactions of the OH adduct with O2 or unimolecular reactions of the peroxy radical (e.g., ring closure), a basic mechanism already proposed previously.^{33–} Four different peroxy radicals can be formed in the OHbenzene adduct + O2 reaction, with O2 in the ortho or para position and syn or anti position with respect to the OH. Theoretical work suggests that a ring-closure reaction is most likely for the peroxy radical with the O2 at the ortho and syn position.²³⁻²⁵ Nevertheless, the presence of other, even unproductive equilibria between the OH adduct and peroxy radicals can influence the kinetics of the adduct loss in the presence of O2. In any case, the apparent second-order rate constant of the adduct + O2 reaction will be an effective one that combines the effects of several elementary reactions. This conclusion also affects the interpretation of the weak temperature dependence of the rate constants for benzene shown in Figure 4 that was considered implausible previously.²² In the simplest case of a fast equilibrium forming a peroxy radical and a comparatively slow subsequent unimolecular reaction of it, the effective second-order adduct + O2 rate constant corresponds to the product of the equilibrium constant and the rate constant of the unimolecular reaction.¹⁹ Accordingly, the opposing temperature dependencies can compensate for each other, resulting in an apparently weak temperature dependence of the effective

adduct $+ O_2$ rate constant. In principle, this applies to other aromatics as well, but an increasing number of possible peroxy radical isomers and competing loss reactions further complicates the situation.

Following the general statements by Vereecken, 28 a likely mechanism of the adduct + O2 reactions for 1245-TeMB-OH is described in the following. The ortho adduct can reversibly form four different peroxy radicals: two with the O2 at the ortho position with respect to OH at a CH3-substituted carbon atom (syn, anti) and two with the O2 bound at the para position with respect to OH at an unsubstituted carbon atom (syn, anti). The peroxy radical with O_2 at the ortho and syn position can undergo 1,3 ring closure at another carbon atom that is CH3-substituted. This ring closure is probably irreversible in the presence of O2 because the bicyclic radicals are scavenged by O2.28 The other peroxy radicals will dissociate back to the ortho adduct + O2, so eventually the complete loss could be channeled through one of the peroxy radicals. The ipso adduct can reversibly form six different peroxy radicals: two with the O2 at the ortho position with respect to OH at an unsubstituted carbon atom (syn, anti), two with the O₂ at the ortho position at a CH₃-substituted carbon atom (syn, anti), and two with the O2 bound at the para position at a CH₃-substituted carbon atom (syn, anti). Irreversible ring-closure reactions can again occur in the two peroxy radicals with O2 at the ortho and syn positions, finally binding unsubstituted and CH3-substituted carbon atoms. All of other peroxy radicals are considered unproductive and will dissociate back to the ipso adduct + O_2 .²⁸

The greater adduct + O₂ rate constants for the ortho adduct compared with the ipso adduct are in qualitative agreement with this mechanism if the primary addition of O₂ and/or the ring-closure reactions are promoted by the presence of CH₃ substitutents. This assumption is supported by the general trends observed for the other monoaromatics. However, despite greater rate constants, the leveling off of the adduct loss rates at $[O_2] > 1 \times 10^{16}$ cm⁻³ occurred at smaller effective loss rates and much smaller O2 concentrations compared with those for benzene and toluene. On the other hand, for *p*-xylene and m-xylene, no leveling off of the rate constants was observed 18 at maximum O_2 concentrations of up to 2×10^{16} cm⁻³. The behavior for 1245-TeMB was therefore unexpected but can be explained qualitatively by the formation of comparatively stable peroxy radical isomers that have no ring-closure option. If a significant fraction of radicals is stored temporarily in such stable intermediates, this can decrease the effective loss rate already at low O₂ concentrations.

These qualitative explanations assume that the OH adduct loss kinetics is pseudo-first-order for a given O₂ concentration and that the OH decays as well as the OH adduct decays are in fact triexponential in accordance with the general mechanism. This may not apply even for the simplified O₂ reaction mechanism outlined above. The poorer fit qualities in the presence of O₂ hint in that direction. If this were the case, the type of data analysis used in this work would no longer be applicable since it is based on analytical solutions presuming the presence of three and not more reactive intermediates. On the other hand, the slightly degraded fit qualities may have other causes. We therefore assume that the obtained effective rate constants are reasonable, but their use should be limited to O_2 concentrations below 1×10^{16} cm⁻³. Nevertheless, it is safe to assume that the atmospheric fate of both adduct isomers is completely dominated by secondary reactions with O2, even though the exact distributions of secondary products remain uncertain.

To elucidate the mechanism for 1245-TeMB in more detail, high-quality theoretical calculations are desirable, ideally combined with an experimental approach using advanced techniques for the detection of intermediates or specific products and numerical data evaluation that can account for more than three intermediate species. The detection of reaction intermediates was successful, for example, in the case of OH-initiated oxidation of toluene, ^{37,38} but it remains rather difficult, particularly if different isomers with the same molecular mass and similar absorption characteristics have to be distinguished. If the full mechanism including peroxy radicals can be constrained to a manageable number of key intermediates with reasonably bounded kinetic properties, the available numerical fit approach may reveal more mechanistic details in a future study.

SUMMARY AND CONCLUSIONS

Reactions of O2 with adducts formed from the reaction of OH radicals with 1245-TeMB were investigated between 299 and 339 K. In this work, we determined for the first time the rate constants of the reactions of O2 with the ortho and ipso isomers of OH adducts of an aromatic compound. The rate constants range between $(4-13) \times 10^{-15}$ and $(0.3-3) \times 10^{-15}$ cm³ s⁻¹ for the ortho and ipso adducts, respectively, dependent on temperature and mechanistic details. Overall, we found a small positive temperature dependence. The rate constants for the ortho isomer of 1245-TeM-OH are greater than those measured previously for OH adducts of benzene, toluene, pxylene, and m-xylene but smaller than those of hexamethylbenzene-OH adducts. This confirms the general trend toward greater rate constants with increasing number of CH₃ substituents. Deviations from the expected linear increase in the adduct loss rates with increasing O2 concentration were identified at O_2 concentrations exceeding about 1×10^{16} cm⁻³. The observed leveling off of the adduct loss rates was described before for benzene and toluene, albeit at O2 concentrations greater by 2 orders of magnitude. This behavior was explained by fast, reversible formation of peroxy radicals resulting in effective second-order adduct + O2 rate constants at low O2 concentrations. The rate constants obtained in this work are interpreted accordingly, i.e., their validity is confined to conditions with low O_2 concentrations (<1 \times 10¹⁶ cm⁻³). On the basis of the current understanding of the mechanism from theoretical studies, the greater adduct $+ O_2$ rate constants and the apparently stronger influence of peroxy radicals for

1245-TeMB compared with other aromatics (except fully methylated hexamethylbenzene) are in qualitative agreement with the stabilizing influence of an increased number of CH_3 substituents on the various radical intermediates. Experimental characterization of intermediates in combination with theoretical work is needed to determine the rate constants for all of the elementary reactions involved and to explore the distribution of products of the reaction under ambient conditions.

ASSOCIATED CONTENT

5 Supporting Information

The Supporting Information is available free of charge at https://pubs.acs.org/doi/10.1021/acsearthspace-chem.1c00230.

Examples of decay rate constants, loss rate constants, and signal ratios as functions of 1245-TeMB concentrations (Figures S1 and S2); other representations of the data in Figure 2 with residuals (Figure S3); Arrhenius plot comparisons with previous results for cases A and B (Figures S4 and S5); O₂ rate constants obtained using all decay curves and associated fit qualities (Table S1); O₂ dependence of the case A and case B fit parameters for 330 K (Figures S6 and S7) (PDF)

AUTHOR INFORMATION

Corresponding Authors

Birger Bohn – Institute of Energy and Climate Research, IEK-8: Troposphere, Forschungszentrum Jülich GmbH, 52428 Jülich, Germany; Email: b.bohn@fz-juelich.de

Cornelius Zetzsch — Multiphase Chemistry Department, Max Planck Institute for Chemistry, 55128 Mainz, Germany; Atmospheric Chemistry Research Unit, University of Bayreuth, 95448 Bayreuth, Germany; orcid.org/0000-0002-8650-5514; Email: cornelius.zetzsch@mpic.de

Authors

Paulo Alarcón – Multiphase Chemistry Department, Max Planck Institute for Chemistry, 55128 Mainz, Germany

Thomas Berkemeier — Multiphase Chemistry Department, Max Planck Institute for Chemistry, 55128 Mainz, Germany; orcid.org/0000-0001-6390-6465

Gerhard Lammel – Multiphase Chemistry Department, Max Planck Institute for Chemistry, 55128 Mainz, Germany; Research Centre for Toxic Compounds in the Environment, Masaryk University, 62500 Brno, Czech Republic; orcid.org/0000-0003-2313-0628

Ulrich Pöschl – Multiphase Chemistry Department, Max Planck Institute for Chemistry, 55128 Mainz, Germany; o orcid.org/0000-0003-1412-3557

Complete contact information is available at: https://pubs.acs.org/10.1021/acsearthspacechem.1c00230

Funding

Open access funded by Max Planck Society.

Notes

The authors declare no competing financial interest.

ACKNOWLEDGMENTS

This work is devoted to the memory of Mario Molina, who made major contributions to the field of atmospheric chemical

kinetics, including the degradation of aromatic compounds. Our work was supported within the joint French–German research project ATMOCHEM funded by the Deutsche Forschungsgemeinschaft (DFG) under Grants ZE 792/6-1 and BO-1580/3-1 and by the Max Planck Gesellschaft. We thank Abraham Horowitz (deceased) for comments on the manuscript and useful discussions.

REFERENCES

- (1) Guenther, A. B.; Jiang, X.; Heald, C. L.; Sakulyanontvittaya, T.; Duhl, T.; Emmons, L. K.; Wang, X. The model of emissions of gases and aerosols from nature version 2.1 (MEGAN2.1): an extended and updated framework for modeling biogenic emissions. *Geosci. Model Dev.* 2012, 5, 1471–1492.
- (2) Velasco, E.; Lamb, B.; Westberg, H.; Allwine, E.; Sosa, G.; Arriaga-Colina, J. L.; Jobson, B. T.; Alexander, M. L.; Prazeller, P.; Knighton, W. B.; Rogers, T. M.; Grutter, M.; Herndon, S. C.; Kolb, C. E.; Zavala, M.; de Foy, B.; Volkamer, R.; Molina, L. T.; Molina, M. J. Distribution, magnitudes, reactivities, ratios and diurnal patterns of volatile organic compounds in the Valley of Mexico during the MCMA 2002 & 2003 field campaigns. *Atmos. Chem. Phys.* **2007**, *7*, 329–353.
- (3) Calvert, J. G.; Atkinson, R.; Becker, K. H.; Kamens, R. M.; Seinfeld, J. H.; Wallington, T. G.; Yarwood, G. *The Mechanisms of Atmospheric Oxidation of Aromatic Hydrocarbons*; Oxford University Press: New York, 2002.
- (4) Volkamer, R.; Jimenez, J. L.; San Martini, F.; Dzepina, K.; Zhang, Q.; Salcedo, D.; Molina, L. T.; Worsnop, D. R.; Molina, M. J. Secondary organic aerosol formation from anthropogenic air pollution: Rapid and higher than expected. *Geophys. Res. Lett.* **2006**, 33, L17811.
- (5) Molina, L. T.; Kolb, C. E.; de Foy, B.; Lamb, B. K.; Brune, W. H.; Jimenez, J. L.; Ramos-Villegas, R.; Sarmiento, J.; Paramo-Figueroa, V. H.; Cardenas, B.; Gutierrez-Avedoy, V.; Molina, M. J. Air quality in North America's most populous city overview of the MCMA-2003 campaign. *Atmos. Chem. Phys.* **2007**, *7*, 2447—2473.
- (6) Wennberg, O. P.; Bates, K. H.; Crounse, J. D.; Dodson, L. G.; McVay, R. C.; Mertens, L. A.; Nguyen, T. B.; Praske, E.; Schwantes, R. H.; Smarte, M. D.; St Clair, J. M.; Teng, A. P.; Zhang, X.; Seinfeld, J. H. Gas-phase reactions of isoprene and its major oxidation products. *Chem. Rev.* **2018**, *118*, 3337–3390.
- (7) Crounse, J. D.; Nielsen, L. B.; Jørgensen, S.; Kjaergaard, H. G.; Wennberg, P. O. Autoxidation of organic compounds in the atmosphere. *J. Phys. Chem. Lett.* **2013**, *4*, 3513–3520.
- (8) Bianchi, F.; Kurtén, T.; Riva, M.; Mohr, C.; Rissanen, M. P.; Roldin, P.; Berndt, T.; Crounse, J. D.; Wennberg, P. O.; Mentel, T. F.; Wildt, J.; Junninen, H.; Jokinen, T.; Kulmala, M.; Worsnop, D. R.; Thornton, J. A.; Donahue, N.; Kjaergaard, H. G.; Ehn, M. Highly oxygenated organic molecules (HOM) from gas-phase autoxidation involving peroxy radicals: a key contributor to atmospheric aerosol. *Chem. Rev.* **2019**, *119*, 3472–3509.
- (9) Atkinson, R. Kinetics and Mechanisms of the Gas-Phase Reactions of the Hydroxyl Radical with Organic Compounds; Journal of Physical and Chemical Reference Data Monograph 1; American Chemical Society and American Institute of Physics, 1989.
- (10) Atkinson, R. Atmospheric chemistry of VOCs and NO_x. Atmos. Environ. **2000**, 34, 2063–2101.
- (11) Berndt, T.; Böge, O. Rate constants for the gas-phase reaction of hexamethylbenzene with OH radicals and H atoms and of 1,3,5-trimethylbenzene with H atoms. *Int. J. Chem. Kinet.* **2001**, 33, 124–129.
- (12) Atkinson, R.; Arey, J. Mechanisms of the gas-phase reactions of aromatic hydrocarbons and PAHs with OH and NO₃ radicals. *Polycyclic Aromat. Compd.* **2007**, *27*, 15–40.
- (13) Loison, J.-C.; Rayez, M.-T.; Rayez, J.-C.; Gratien, A.; Morajkar, P.; Fittschen, C.; Villenave, E. Gas-phase reaction of hydroxyl radical with hexamethylbenzene. *J. Phys. Chem. A* **2012**, *116*, 12189–12197.

- (14) Aschmann, S. M.; Arey, J.; Atkinson, R. Rate constants for the reactions of OH radicals with 1,2,4,5-tetramethylbenzene, pentamethylbenzene, 2,4,5-trimethylbenzaldehyde, 2,4,5-trimethylphenol, and 3-methyl-3-hexene-2,5-dione and products of OH + 1,2,4,5-tetramethylbenzene. *J. Phys. Chem. A* **2013**, *117*, 2556–2568.
- (15) Alarcón, P.; Bohn, B.; Zetzsch, C. Kinetic and mechanistic study of the reaction of OH radicals with methylated benzenes: 1,4-dimethyl-, 1,3,5-trimethyl-, 1,2,4,5-, 1,2,3,5- and 1,2,3,4-tetramethyl-, pentamethyl-, and hexamethylbenzene. *Phys. Chem. Chem. Phys.* **2015**, 17, 13053–13065.
- (16) Wahner, A.; Zetzsch, C. Rate constants for the addition of OH to aromatics (benzene, p chloroaniline, and *o-, m-,* and p-dichlorobenzene) and the unimolecular decay of the adduct. Kinetics into a quasi-equilibrium. *J. Phys. Chem.* **1983**, 87, 4945–4951.
- (17) Knispel, R.; Koch, R.; Siese, M.; Zetzsch, C. Adduct formation of OH-radicals with benzene, toluene, and phenol and consecutive reactions of the adducts with NO_X and O₂. *Ber. Bunsenges. Phys. Chem.* **1990**, *94*, 1375–1379.
- (18) Koch, R.; Knispel, R.; Elend, M.; Siese, M.; Zetzsch, C. Consecutive reactions of aromatic-OH adducts with NO, NO₂ and O₂: benzene, naphthalene, toluene, *m* and *p*-xylene, hexamethylbenzene, phenol, *m*-cresol and aniline. *Atmos. Chem. Phys.* **2007**, *7*, 2057–2071
- (19) Bohn, B.; Zetzsch, C. Gas-phase reaction of the OH-benzene adduct with O₂: reversibility and secondary formation of HO₂. *Phys. Chem. Chem. Phys.* **1999**, *1*, 5097–5107.
- (20) Bohn, B. Formation of peroxy radicals from OH-toluene adducts and O₂. J. Phys. Chem. A 2001, 105, 6092-6101.
- (21) Johnson, D.; Raoult, S.; Rayez, M.-T.; Rayez, J.-C.; Lesclaux, R. An experimental and theoretical investigation of the gas-phase benzene–OH radical adduct + O₂ reaction. *Phys. Chem. Chem. Phys.* **2002**, *4*, 4678–4686.
- (22) Grebenkin, S. Y.; Krasnoperov, L. N. Kinetics and thermochemistry of the hydroxycyclo-hexadienyl radical reaction with O_2 : $C_6H_6OH + O_2 = C_6H_6(OH)OO$. *J. Phys. Chem. A* **2004**, 108, 1953–1963.
- (23) Raoult, S.; Rayez, M.-T.; Rayez, J.-C.; Lesclaux, R. Gas phase oxidation of benzene: Kinetics, thermochemistry and mechanism of initial steps. *Phys. Chem. Chem. Phys.* **2004**, *6*, 2245–2253.
- (24) Glowacki, D. R.; Wang, L.; Pilling, M. J. Evidence of formation of bicyclic species in the early stages of atmospheric benzene oxidation. *J. Phys. Chem. A* **2009**, *113*, 5385–5396.
- (25) Olivella, S.; Solé, A.; Bofill, J. M. Theoretical mechanistic study of the oxidative degradation of benzene in the troposphere: reaction of benzene-HO radical adduct with O₂. *J. Chem. Theory Comput.* **2009**, *5*, 1607–1623.
- (26) Uc, V. H.; Garcia-Cruz, I.; Hernandez-Laguna, A.; Vivier-Bunge, A. New channels in the reaction mechanism of the atmospheric oxidation of toluene. *J. Phys. Chem. A* **2000**, *104*, 7847–7855.
- (27) Suh, I.; Zhang, D.; Zhang, R.; Molina, L. T.; Molina, M. J. Theoretical study of OH addition reaction to toluene. *Chem. Phys. Lett.* **2002**, 364, 454–462.
- (28) Vereecken, L. Reaction mechanisms for the atmospheric oxidation of monocyclic aromatic compounds. In *Advances in Atmospheric Chemistry*; World Scientific, 2019; pp 377–527.
- (29) Bohn, B.; Zetzsch, C. Kinetics and mechanism of the reaction of OH with the trimethylbenzenes experimental evidence for the formation of adduct isomers. *Phys. Chem. Chem. Phys.* **2012**, *14*, 13933–13948.
- (30) Alarcon, P.; Strekowski, R.; Zetzsch, C. Reversible addition of the OH radical to *p*-cymene in the gas phase: kinetic analysis assuming formation of a single adduct. Part 1. *Phys. Chem. Chem. Phys.* **2013**, *15*, 20105–20114.
- (31) Davison, A. C.; Hinkley, D. V. Bootstrap Methods and Their Application; Cambridge University Press: Cambridge, U.K., 1997.
- (32) Berkemeier, T.; Ammann, M.; Krieger, U. K.; Peter, T.; Spichtinger, P.; Pöschl, U.; Shiraiwa, M.; Huisman, A. J. Technical note: Monte Carlo genetic algorithm (MCGA) for model analysis of

- multiphase chemical kinetics to determine transport and reaction rate coefficients using multiple experimental data sets. *Atmos. Chem. Phys.* **2017**, *17*, 8021–8029.
- (33) Atkinson, R.; Lloyd, A. C. Evaluation of kinetic and mechanistic data for modeling of photochemical smog. *J. Phys. Chem. Ref. Data* **1984**, *13*, 315–444.
- (34) Bartolotti, L. J.; Edney, E. O. Density functional theory derived intermediates from the OH initiated atmospheric oxidation of toluene. *Chem. Phys. Lett.* **1995**, 245, 119–122.
- (35) Lay, T. H.; Bozzelli, J. W.; Seinfeld, J. H. Atmospheric photochemical oxidation of benzene: benzene + OH and the benzene-OH adduct (hydroxyl-2,4-cyclohexadienyl) + O₂. *J. Phys. Chem.* **1996**, 100, 6543–6554.
- (36) Suh, I.; Zhang, R.; Molina, L. T.; Molina, M. J. Oxidation mechanism of aromatic peroxy and bicyclic radicals from OH–toluene reactions. *J. Am. Chem. Soc.* **2003**, *125*, 12655–12665.
- (37) Molina, M. J.; Zhang, R.; Broekhuizen, K.; Lei, W.; Navarro, R.; Molina, L. T. Experimental study of intermediates from OH-initiated reactions of toluene. *J. Am. Chem. Soc.* **1999**, *121*, 10225–10226.
- (38) Birdsall, A. W.; Andreoni, J. F.; Elrod, M. J. Investigation of the role of bicyclic peroxy radicals in the oxidation mechanism of toluene. *J. Phys. Chem. A* **2010**, *114*, 10655–10663.